Research Square

Preprints are preliminary reports that have not undergone peer review.
They should not be considered conclusive, used to inform clinical practice,
or referenced by the media as validated information.

AAV8-PDE6B with 3'UTR provides durable rescue of photoreceptor structure and function in rd10 mouse model of retinitis pigmentosa

Steven S. Eamegdool
Children's Medical Research Institute
To Ha Loi
Children's Medical Research Institute
Amin Sabri
Children's Medical Research Institute
Fidelle Chahine Karam
Children's Medical Research Institute
Anson Cheng
Children's Medical Research Institute
Leszek Lisowski
Children's Medical Research Institute
John R. Grigg
Children's Medical Research Institute
Ian Alexander
Children's Medical Research Institute
Robyn V. Jamieson
rjamieson@cmri.org.au

Children's Medical Research Institute

Research Article

Keywords:

Posted Date: May 20th, 2026

DOI: https://doi.org/10.21203/rs.3.rs-9298568/v1

License: This work is licensed under a Creative Commons Attribution 4.0 International License.
Read Full License

Additional Declarations: No competing interests reported.

AAV8-*PDE6B* with 3'UTR provides durable rescue of photoreceptor structure and function in *rd10* mouse model of retinitis pigmentosa

Steven S. Eamegdool[1], To Ha Loi[1], Amin Sabri[1], Fidelle Chahine Karam[1], Anson Cheng[1], Leszek Lisowski[2,3,4,5], John R. Grigg[1,6], Ian Alexander[7], Robyn V. Jamieson[1,8,9,*]

[1]Eye Genetics Research Unit, Children's Medical Research Institute, Sydney, Australia

[2]Vector and Genome Engineering Facility, Children's Medical Research Institute, Sydney, Australia

[3]Translational Vectorology Research Unit, Children's Medical Research Institute, Faculty of Medicine and Health, The University of Sydney, Sydney Australia

[4]Laboratory of Molecular Oncology and Innovative Therapies, Military Institute of Medicine – National Research Institute, Warsaw, Poland

[5]Australian Genome Therapeutics Centre, Children's Medical Research Institute, Sydney Children's Hospitals Network, Sydney, Australia

[6]Save Sight Institute and Specialty of Ophthalmology, Faculty of Medicine and Health, University of Sydney, Sydney, Australia

[7]Gene Therapy Research Unit, Children's Medical Research Institute, Sydney, Australia

[8]Department of Clinical Genetics, Western Sydney Genetics Program, Sydney Children's Hospitals Network, Sydney, Australia

[9]Specialty of Genomic Medicine, Faculty of Medicine and Health, University of Sydney, Sydney, Australia

*Correspondence: rjamieson@cmri.org.au

Abstract

Retinitis pigmentosa (RP), a leading cause of inherited blindness, often results from phosphodiesterase 6 (PDE6) deficiency. We evaluated a novel gene therapy construct, AAV8-RK-PDE6B-3'UTR, in the *rd10* mouse model which lacks the functional β-subunit of PDE6. The construct utilises a rhodopsin-kinase promoter, human PDE6B cDNA, and a PDE6B 3' untranslated region (3'UTR), which was delivered subretinally at postnatal day 12 (P12). Treated mice showed sustained preservation of retinal function and structure for up to 15 months, as confirmed by visual acuity (VA), electroretinography (ERG), optical coherence tomography (OCT), and immunohistochemistry. This represents the first demonstration of such long-term rescue in this model. These data indicate that the combination described here of vector capsid type and promoter specific to photoreceptors, along with *PDE6B* 3'UTR sequence provides benefit in longevity of therapeutic effect in *PDE6B* gene therapy.

Introduction

Retinitis pigmentosa (RP) encompasses a group of inherited retinal diseases (IRDs) characterised by progressive rod photoreceptor degeneration and subsequent cone photoreceptor loss. RP usually manifests early with night blindness, followed by deterioration of peripheral vision and may progress towards complete blindness. Approximately 4-5% of cases of RP are due to pathogenic variants affecting subunits of the rod phosphodiesterase 6 complex (PDE6), with most affecting the beta-subunit and leading to autosomal recessive *PDE6B*-related RP (OMIM:180072)[1, 2]. A variety of loss-of-function disease-causing variants in *PDE6B* are reported including those with nonsense, frameshift, splice-site or missense molecular consequences[3]. Loss-of-function of PDE6B leads to toxic accumulation of cyclic guanosine monophosphate (cGMP) and elevated intracellular calcium-mediated cell death[4, 5]. Mouse models of *PDE6B* RP have proven useful in examination of disease pathophysiology and testing of therapy approaches. In the *rd10* mouse line, with a homozygous pathogenic missense variant in exon 13 of mouse *Pde6b*, retinal degeneration occurs after 2 weeks of postnatal life, providing useful timing for testing therapeutic efficacy and duration[6, 7].

In IRDs, gene therapy interventions have occurred predominantly through viral-mediated delivery of the therapeutic construct, with adeno-associated viruses (AAVs) being the most common delivery vehicle[8]. AAV8, a serotype originally isolated from rhesus monkey, was found to be effective at transducing photoreceptors and retinal pigment epithelial (RPE) cells more efficiently than AAV2 and AAV5 following subretinal injection into non-degenerate mouse eyes[9, 10]. While several serotypes

(AAV2, 5, and 8) are in human therapy and clinical trial studies for IRDs, achieving long-term stable expression remains a challenge[11-13]. Strategies to improve transduction and contribute to long term efficacy include optimisation of the size of the cassette and use of cell-specific promoters [11, 14]. Regulatory elements, including those that are gene-specific, may also contribute to sustained therapeutic efficacy[15, 16]. While impact of forms of *PDE6B* gene replacement therapy have been shown in the rd10 mouse[14] and a dog model[17], and a now terminated clinical trial reported short term safety[18], there are considerations concerning durability of genetic therapy strategies in the eye, highlighting potential benefits of alternative designs[19, 20].

In this study, we report the use of a novel *PDE6B* gene therapy vector construct in an *rd10* mouse model of RP, with *PDE6B* 3'UTR sequence in the construct. We found that our vector construct led to sustained long-term preservation (up to 15 months) of rod and cone photoreceptors, as well as stable expression of PDE6B in these cells, with no adverse inflammatory reactions detected within the retina. In addition, retinal structure and visual function was maintained over this period indicative of successful and sustained therapeutic intervention.

Materials and Methods

Animals

C57BL/6 (Animal Resources Centre, Western Australia) and *rd10* (Jackson Labs, ME, US) mice were used. All animal procedures were approved by the Children's Medical Research Institute Animal Ethics Committee (Project C205).

Creation of AAV therapy constructs and controls

A segment of the human rhodopsin kinase (RK, *GRK1*) promoter (-112 to +183, GenBank: AY327580.1), and the human *PDE6B* cDNA (NM_000283.3, isoform 1), with Kozak sequence directly before the ATG start codon, were synthesised by Genscript Biotech (Singapore) for cloning. The recipient plasmid pAAV2 ITR 2336v2, which has an optimised backbone ready for clinical AAV vector production, was supplied by Dr Sharon Cunningham (CMRI, Westmead, Australia) and modified as follows. The original promoter sequence was replaced with the RK promoter -112 to +183 using PacI and NotI restriction enzymes (NEB, MA, USA). The plasmid was then digested with HpaI and SalI (NEB), to remove the original cDNA and insert in its place the human *PDE6B* cDNA sequence, after the RK promoter but separated by an SV40 intron element. Following this, for the first construct, the *PDE6B* 3'UTR sequence was PCR amplified from normal human genomic DNA using primers with a SalI restriction enzyme site and subsequently cloned into SalI digested plasmid, directly after the *PDE6B* cDNA, and followed by bovine growth hormone polyA sequence (bGHpA) (Figure 1A). Two other constructs containing the RK promoter and *PDE6B* cDNA were created, one without the 3'UTR and one with the 3'UTR replaced by GFP. A fourth construct contained the RK promoter with GFP and 2503 bp of non-coding stuffer

sequence[21, 22]. A fifth construct contained a CMV promoter and GFP sequences (Vector and Genome Engineering Facility, CMRI, Westmead, Australia). The entire expression cassettes in all final constructs produced were verified by Sanger sequencing (Australian Genome Research Facility, AGRF, Westmead, Australia). All plasmid propagations were performed using One Shot Stbl3 competent cells (Thermofisher, MA, USA). For AAV vector production, each construct was packaged in standard AAV2 serotype 8 (AAV2/8, hereby referred to in this paper as AAV8) capsids and viral particles were purified using CsCl ultracentrifugation (Vector and Genome Engineering Facility, CMRI, Westmead, Australia)[23]. The AAV vectors were called, respectively: AAV8-RK-PDE6B-3'UTR, AAV8-RK-PDE6B, AAV8-RK-PDE6B-GFP, AAV8-RK-GFP-pA-stuffer, AAV8-CMV-GFP (Figure 1A).

Cellular testing of AAV vectors

Preliminary screening for *PDE6B* expression capacity of each AAV vector construct was performed *in vitro* using a mouse photoreceptor cell line, 661W (kindly provided by Prof Muayyad R. Al-Ubaidi, University of Houston, TX, USA)[24]. This cell line lacked endogenous expression of murine *Pde6b* (data not shown), and a human-specific primer pair was used to detect exogenous *PDE6B* expression, driven by the RK promoter, following transduction. 661W cells were seeded into a 24-well plate at 2.5×10^4 cells/mL and incubated for 24 hr in DMEM/10% FBS. Subsequent evaluation of AAV transduction efficiency in these cells, via immunohistochemistry and flow-cytometry, were performed similarly to Wagner *et al* [25]. The cells were transduced with different AAV constructs at 1×10^6 multiplicity of infection (MOI) for 72 hours. Following this, the cells were either fixed in 4% paraformaldehyde at 4 °C for 20 min (for

immunohistochemistry and flow-cytometry) or flash-frozen (for RT-qPCR (QPCR) analysis).

For immunohistochemistry, cells were permeabilised with 0.1% Triton X-100/PBS for 30 min, room temperature, followed by blocking in 5% BSA/0.1% Triton X-100/PBS for 30 min, room temperature, and incubated with primary antibodies, made up in 1% BSA/0.1% Triton X-100/PBS, for 16 h, 4 ºC. The antibodies used were as follows: PDE6B (rabbit IgG; 1:200) (ThermoFisher); or anti-GFP (rabbit IgG; 1:500) (ThermoFisher). Immune complexes were detected with secondary donkey antibodies (1:500) (2 hr, room temperature) to rabbit IgG, labelled with Alexa-Fluor 488 (ThermoFisher). Nuclei were counterstained with Hoechst 33258 (1:10,000) prior to mounting in glycerol:PBS (80:20) and slides were sealed with nail varnish. All images were captured using an LSM 880 Meta Confocal microscope system and ZEN Blue software (Carl Zeiss, Oberkochen Germany). Images were assembled in Photoshop CS software (Adobe Corporation, CA, USA).

For flow-cytometry, cells were pelleted and prepared for antibody staining as mentioned above. Primary and secondary antibody incubation times were 1 hr, 4 ºC, each. Flow-cytometric analysis and quantification was performed using a BD FACSCanto (BD Biosciences, NJ, USA).

For RNA analysis, total RNA was extracted using the RNAeasy micro kit (Qiagen, MD, USA), followed by cDNA conversion using SuperScript IV 1st Strand Synthesis kit (Invitrogen, MA, USA). Relative gene expression was determined via 1 × SensiMix

SYBR (Bioline, NSW, Australia) on a Rotor-Gene 6000 Cycler system (Qiagen). Markers used for QPCR studies were as follows: *PDE6B* (human)*, Polr2a* (*RNA pol*) (mouse). Relative gene expression was calculated by the $2^{-\Delta CT}$ analysis compared to the expression of housekeeping gene *RNA pol*. Primers were designed using PrimerBlast and synthesised by Sigma-Aldrich (Sigma-Aldrich, MO, USA) (Table S1).

Subretinal injections

P12 *rd10* mice were anaesthetised by intraperitoneal injection of a mixture of ketamine (100 mg/kg) and xylazine (10 mg/kg), followed by application of 0.5% tropicamide eye drop. An incision in the pars plana region of the sclera was made with the help of a 30G needle and subretinal injections were carried out with a 34G Hamilton syringe (Hamilton) using 1.8 x 10^{10} genome copies (GC) of AAV vector in an injection volume of 1 µL. Subretinal injections were performed on the right eye of the animal in the superior-nasal location using an ophthalmic surgical microscope (Carl Zeiss), and the fellow left eye was not injected. The condition in which the eye received the AAV8-RK-PDE6B-3'UTR injection was designated as "Treated", while the fellow un-injected left eye was referred to as "Untreated". Wild-type C57Bl/6 with no injection given was designated as the "Control" condition. Following injections, ophthalmic lubricant ointment (Systane, Alcon, USA) was given and recovery was monitored over 1 week. At designated timepoints after subretinal injections, including 1, 2, 6, 9, 12 and 15 months, animals underwent phenotypic and functional vision assessment or were euthanised via cervical dislocation, and eyes were enucleated and prepared for immunohistochemical analysis.

Optomotor testing

Photopic visual acuity and contrast sensitivity of AAV8-RK-PDE6B-3'UTR treated and untreated rd10 eyes were measured using an optomotor test system (OptoMotry, Cerebral Mechanics Inc, NY, USA). Thresholds for each eye were determined simultaneously via stepwise functions for correct responses in both the clockwise and counter-clockwise direction. Acuity was defined as the highest spatial frequency (100% contrast) yielding a threshold response. The initial stimulus was 0.200 cyc/deg sinusoidal pattern with a fixed 100% contrast. All patterns were presented at a speed of 12 degrees per second. Visual acuity was measured for both eyes of the mice the day before performing ERG. The results from the fellow non-injected left eye of the *rd10* mice was the same as those *rd10* mice that received no treatment, therefore conditions that were designated "Untreated" are from the fellow left eye.

Electroretinography

Full-field, flash ERGs were collected from the mice post injection, using a Phoenix Micron® Ganzfeld ERG test system (Micron IV, Phoenix Technology Group, CA, USA). Mice were dark adapted overnight, and rod responses and mixed rod/cone responses were generated using -1.7, -0.8, 0.1, 1, 1.9, 2.8 and 3.1 log cd·s/m^2 (scotopic) broadband light stimulus respectively (see Table S2 for parameters).

Afterwards, the mice were light adapted by exposure to a steady UV light (3.1 log cd·s/m^2) for 5 min, followed by acquisition of cone-isolated responses to 0.1, 1, 1.9, 2.8 and 3.1 log cd·s/m^2 (photopic) broadband UV light stimulus respectively (see Table S3 for parameters).

205

206 **Optical coherence tomography**

207 Retinal integrity was monitored via Optical Coherence Tomography (OCT) and
208 fundoscopy (Micron IV, Phoenix Technology Group). For “Control” and “Untreated”
209 conditions, OCT scans were taken at multiple locations across the retina so that the
210 inferior and superior regions could be measured. For the “Treated” condition, typical
211 coverage of the injection was in the superior-nasal region encompassing 1/3 of the
212 whole retina, thus measurements were taken only from this region, unless otherwise
213 stated, to measure the effectiveness of the AAV construct and treatment. Using
214 Insight2D image segmentation software, measurements were made from the ganglion
215 cell layer (GCL) to the RPE to measure total retinal thickness since retinal thickness
216 measurements obtained via OCT correlate well with measurements from *ex vivo*
217 histology[26].

218

219 **Immunohistochemistry**

220 AAV8-RK-PDE6B-3’UTR treated and untreated eyes were fixed in 4%
221 paraformaldehyde at 4 °C for 1 hr, then cryo-protected with 30% sucrose solution and
222 embedded in OCT solution (Tissue Tek, CA, USA). Sections were cut at 14 µm
223 thickness. Sections were permeabilised with 0.1% Triton X-100/PBS for 30 min, room
224 temperature, followed by blocking in 5% BSA/0.1% Triton X-100/PBS for 30 min, room
225 temperature, and incubated with primary antibodies, made up in 1% BSA/0.1% Triton
226 X-100/PBS, for 16 h, 4 ºC. The antibodies used were as follows: specific for astrocytes
227 and activated Müller glia: GFAP-Cy3 conjugate (mouse IgG; 1:800) (Sigma-Aldrich);
228 microglia: Iba1 (rabbit IgG; 1:500) (Wako, Osaka, Japan); cone photoreceptors: cone

arrestin (rabbit IgG; 1:200) (Merck Millipore, MA, USA), rod photoreceptors: rhodopsin (mouse IgG; 1:200) (Merck Millipore); rod bi-polar cells: PKCα (mouse IgG; 1:100) (ThermoFisher); PDE6B (rabbit IgG; 1:200) (ThermoFisher); and cGMP (sheep IgG; 1:300) (gifted by Prof Steinbusch and Dr De Vente, Maastricht University, The Netherlands). Immune complexes were detected with secondary donkey antibodies (1:500) (2 hr, room temperature) to sheep IgG, mouse IgG, or rabbit IgG, labelled with Alexa-Fluor 488, 555, or 647 (ThermoFisher). Nuclei were counterstained with Hoechst 33258 (1:10,000) prior to mounting in glycerol:PBS (80:20) and slides were sealed with nail varnish. All images were captured using an LSM 880 Meta Confocal microscope system and ZEN Blue software (Carl Zeiss). Images were assembled in Photoshop CS software (Adobe Corporation).

Injection of the AAV construct in the treated condition typically encompasses 1/3 of the whole retina in the supero-nasal region, thus all measurements were performed in this region, unless otherwise stated. The mean number of $Iba1^+$ cells was calculated from 3 fields of view (FOV) within the retina (n = 5 eyes/condition) and normalised to tissue retina area (cells/mm^2). For cone measurements, the number of cones were calculated from 3 FOV within the retina (n = 5 eyes/condition) and normalised to 100 µm retinal length. PDE6B, cGMP, GFAP and PKCα immnolabelling density was calculated using the 'Threshold' option in ImageJ (NIH,USA), with the scale set to pixels to derive the value of pixels within the FOV prior to normalisation to tissue area (pixel/$µm^2$)[27]. The mean density was calculated from 3 FOV for each condition (n = 5 eyes/condition).

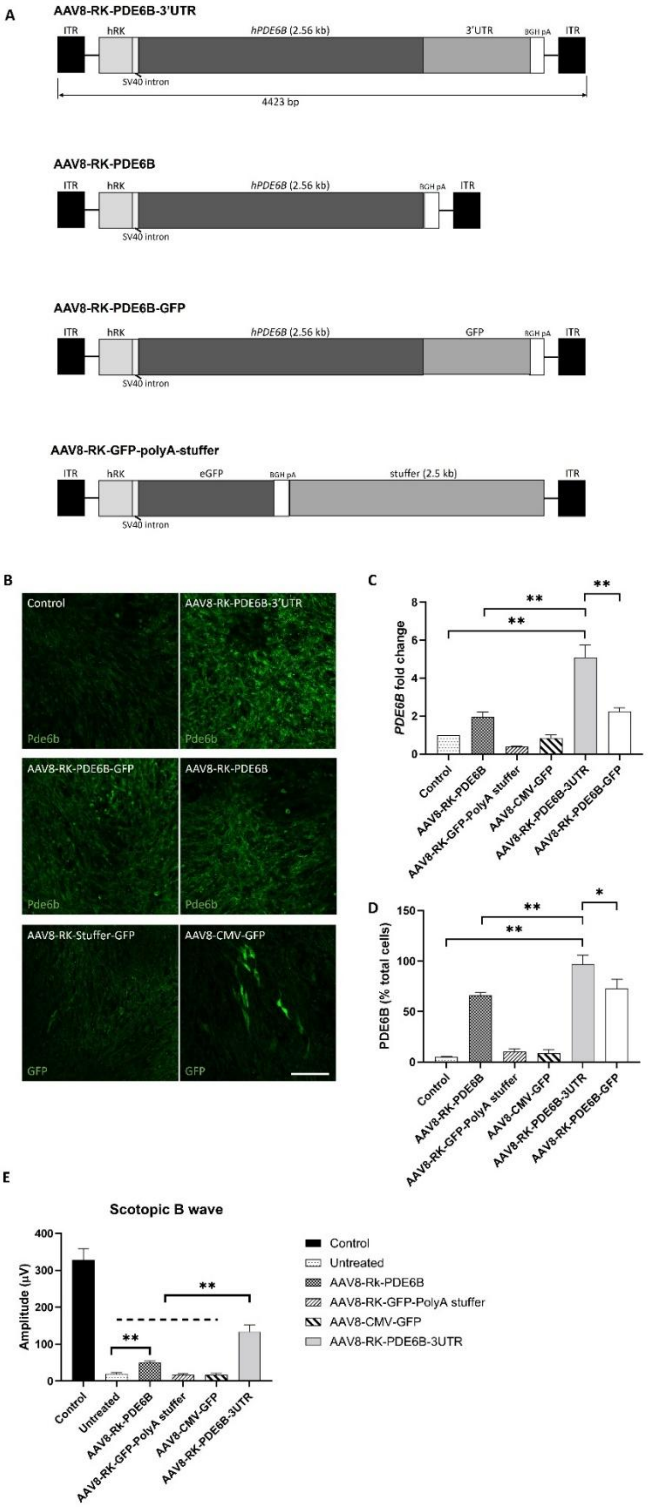
Statistical analysis

Data was expressed as mean ± standard error of the mean (SEM) with sample size (n) Significance was determined between the average of two groups using One-way ANOVA with Tuey's post-hoc test. An alpha value of 5% ($p < 0.05$) was considered statistically significant and indicated in the figures as * ($p < 0.05$) or ** ($p < 0.01$) where appropriate. Statistical analysis was performed using GraphPad Prism 6.0 (GraphPad software, MA, USA) for Windows.

Results

AAV8-RK-PDE6B-3'UTR provided greater PDE6B expression in cells and *rd10* mice

The human PDE6B cDNA (Figure 1A), inclusive of the 3' UTR region, driven by the human rhodopsin kinase promoter, was incorporated into a construct that was packaged into a recombinant AAV8 vector. The efficacy of this vector was then tested and screened against other vectors without the specific 3' UTR region via *in vitro* expression assays in a 661W mouse photoreceptor cell line (Figure 1B). Cells which were transduced with the AAV8-RK-PDE6B-3'UTR vector displayed significantly higher expression of PDE6B, both at the RNA (Figure 1C) and protein levels (Figure 1D), compared with other constructs including the similar length construct with GFP instead of the PDE6B 3'UTR and the shorter construct with only the RK promoter and PDE6B cDNA. After the initial *in vitro* screening, the AAV8-RK-PDE6B-3'UTR vector was then subretinally delivered into the right eye of *rd10* mice. We also initially screened and validated our AAV8-RK-PDE6B-3'UTR construct *in vivo* by comparing against other AAV constructs, via ERG measurements in *rd10* mice at one month-post injection, to corroborate with the *in vitro* efficacy assessment (Figure 1E). We found that our AAV8-RK-PDE6B-3'UTR construct provided superior rescue (photopic B-wave response) compared to other constructs.



280

281 **Figure 1: Screening expression efficacy of AAV8-RK-PDE6B-3'UTR vector *in***
282 ***vitro* and *in vivo*.** (A) Outline of AAV vector cassettes used to express the *PDE6B*
283 gene. Expression was driven by the human rhodopsin kinase (hRK), with a polyA
284 bovine growth hormone (BGH pA) regulatory region at the 3'-end of the *PDE6B*

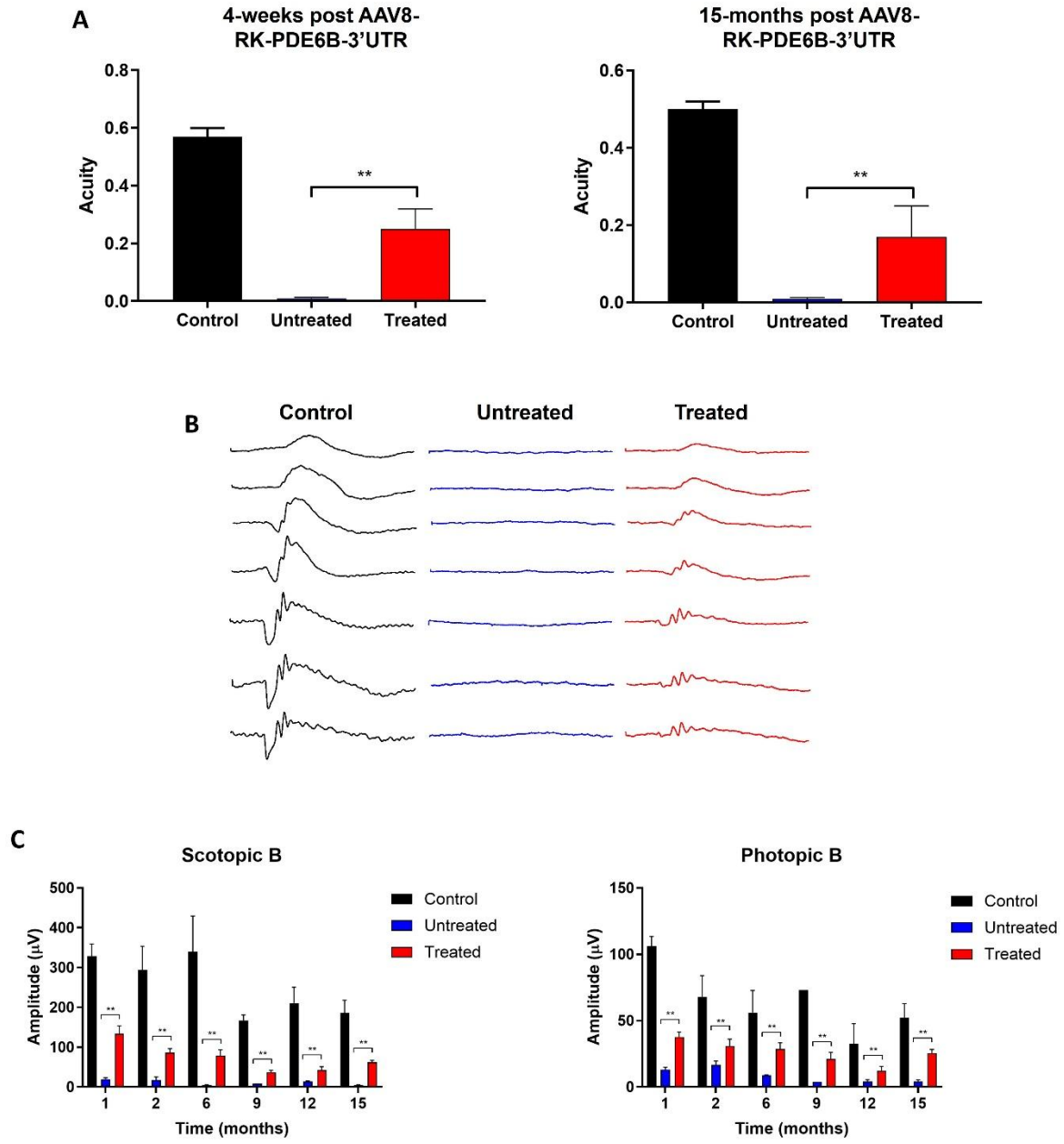
sequence. (B) Representative images of 661W cells transduced with various vectors. Cells transduced with the AAV8-PDE6B-3UTR vector showed prominent PDE6B staining compared to the control condition as well as other vectors. Scale bar = 50 μm. This effect was quantified via both: (B) QPCR, and (C) flow-cytometry, whereby conditions with the AAV8-RK-PDE6B-3'UTR vector displayed significantly more PDE6B expression. Significance relative to control untransduced conditions (n = 3) is indicated as: *, $p < 0.05$ or **, $p < 0.01$. Error bar represents standard error mean. (D) Average scotopic B-wave amplitudes elicited at 1.9 log cd.s/m^2 in age-matched eyes (1 month post-injection) in various conditions. AAV8-RK-PDE6B vector showed some rescue effect when compared with non-treated eyes. AAV8-RK-GFP-PolyA stuffer vector did not show a rescue effect. AAV8-CMV-GFP did not cause a non-specific rescue effect. The AAV8-RK-PDE6B-3'UTR vector displayed significantly better rescue effect than all the other vectors, emphasising the value of the 3'UTR region in the construct. Significance relative to Untreated eyes, and eyes that received other AAV vectors (n = 3), is indicated as: **, $p < 0.01$. Error bar represents standard error mean.

AAV8-RK-PDE6B-3'UTR restored retinal function over the long-term

To evaluate longevity of the construct-mediated functional rescue, the Control, Untreated, and Treated eyes were followed up at 2 and 15 months. At 2 months post-injection of the AAV8-RK-PDE6B-3'UTR vector, optomotor behavioural analysis revealed that the treated right eye of *rd10* mice responded significantly better than the untreated left eye (Figure 2A). This was also observed 15 months post-injection, with the rescued right eye of *rd10* mice still showing significantly better responses than the

untreated eye (Figure 2A). As expected, since only approximately one-third of the retina was treated, the wild-type C57Bl/6 eyes (Control) showed better responses than both conditions.

The retinal function of treated *rd10* mice was examined via ERG. In all scotopic tests, untreated eyes had poor ERG signals, equivalent to a lack of rod-mediated visual function, in contrast to rescued scotopic ERGs (in treated eyes) which exhibited presence of A-wave structure and average B-wave amplitudes (Figure 2B). At 1, 2, 6, 9, 12 and 15 months post-injection the rescue effect of the AAV8-RK-PDE6B-3'UTR was evident in both scotopic and photopic measurements (Figure 2C), indicating both rod and cone photoreceptor rescue.



320

321 **Figure 2: AAV8-RK-PDE6B-3'UTR restores visual acuity and preserve retinal**
322 **function in *rd10* eyes.** (A) Untreated *rd10* eyes displayed poor visual acuity
323 compared to Control condition, using an optomotor test system (OptoMotry, Cerebral
324 Mechanics Inc, USA). Delivery of the AAV8-RK-PDE6B-3'UTR therapy construct in
325 the Treated condition resulted in significant recovery in visual acuity of the mice from
326 2 months post-injection up to 15 months post-injection. (B) Representative scotopic B-
327 wave ERG traces recorded from -1.7 log cd.s/m^2 (upper trace) to 3.1 log cd.s/m^2 (lower

trace) over a 300 ms time period, for Control, Untreated, and Treated conditions, at 15 months. (C) Average scotopic and photopic B-wave amplitudes elicited at 1.9 log cd.s/m^2 in age-matched Control, Untreated and Treated eyes (1, 2, 6, 9, 12, 15 months post-injection). AAV8-RK-PDE6B-3'UTR mediated gene therapy showed rescue effects from 1 month up to 15 months post-injection. Significance relative to Untreated eyes (n = 5) is indicated as: **, $p < 0.01$. Error bar represents standard error mean (Control: C57Bl/6 with no injection; Untreated: rd10 with no injection; Treated: rd10 with AAV8-RK-PDE6B-3'UTR injection).

Retinal structure was preserved in AAV8-RK-PDE6B-3'UTR treated *rd10* eyes

Gene augmentation therapy using the AAV8-RK-PDE6B-3'UTR vector stably preserved the retinal structure in *rd10* mice, as observed through fundoscopy and OCT imaging. Fundoscopy revealed that retinal preservation was prominent in the treated *rd10* mouse eyes, as opposed to the untreated eyes which exhibited prominent retinal degeneration over time (Figure 3A). The effects were compared to the wild-type C57Bl/6 mouse eyes.

Retinal layer thickness was measured via images collected *in vivo* using OCT imaging (Figure 3A), and as mentioned in the Methods section; measurements in the Treated condition were taken from areas of photoreceptor rescue as typical coverage of the injection, in the superior-nasal region, encompassed 1/3 of the whole retina, thus measurements were taken only from this region. OCT examination revealed that the retinal structure and morphology was largely maintained in treated regions of the eyes compared to untreated eyes, with the outer nuclear layer (ONL) of treated eyes being

significantly thicker than untreated eyes at all timepoints over the 15 months post-injection (Figure 3B).

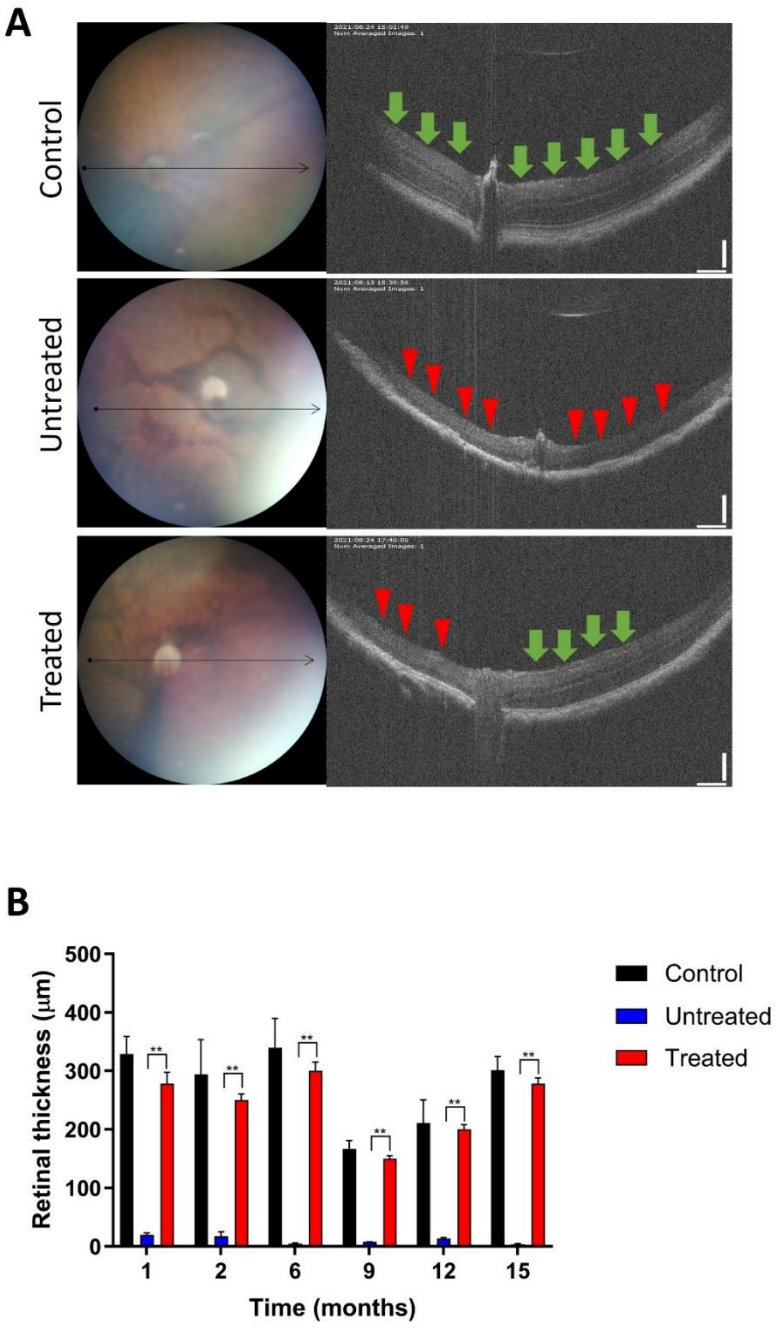


Figure 3: *In vivo* imaging shows structural rescue in treated *rd10* eyes. (A) Bright-field fundoscopy images of Control, Untreated and Treated retina from representative mice at the15 the months post-injection timepoint. Corresponding OCT images are displayed alongside, with Untreated retina displaying clear retinal thinning and

absence of the photoreceptor layer (red arrowheads), compared to Control retina (green arrows). Treated retina (AAV8-RK-PDE6B-3'UTR) contained areas of photoreceptor rescue, along with maintenance of the retinal layer and structure (green arrows), compared with non-injected areas (red arrowheads). Scale bar = 50 μm. (B) In the treated retina, rescue of photoreceptors and retinal thickness persisted up to the 15 month post-treatment time period. Significance relative to Untreated eyes (n = 5) is indicated as: **, $p < 0.01$. Error bar represents standard error mean (Control: C57Bl/6 with no injection; Untreated: rd10 with no injection; Treated: rd10 with AAV8-RK-PDE6B-3'UTR injection).

PDE6B expression observed in rescued photoreceptors of AAV8-RK-PDE6B-3'UTR treated *rd10* mice

To determine the effects of AAV8-RK-PDE6B-3'UTR treatment we phenotypically characterised and quantified the proportion of photoreceptors rescued, and PDE6B expressed, using immunohistochemistry. It was found that photoreceptors were maintained at 4 weeks after AAV8-RK-PDE6B-3'UTR injection, and this therapeutic rescue persisted up to 15 months post-treatment. In control C57Bl/6 retina, PDE6B was expressed in the photoreceptor layer outer segment, where it was co-expressed with rhodopsin (Figure 4A). This was also observed in treated *rd10* retina (Figure 4A). However, in untreated *rd10* retina, no rhodopsin-positive photoreceptors were present and minimal PDE6B expression was observed, indicative of significant photoreceptor degeneration (Figure 4A). Treatment with AAV8-RK-PDE6B-3'UTR conveyed a clear therapeutic effect that was observed at 4 weeks post-treatment (Figure 4C), and maintained up to 15 months post-injection, within sustained PDE6B expression

intensity over that time (Figure 4B and D). Photoreceptor rescue was localised to the area of the injection site (Figure 4E, green arrows), with no rescue effects seen further away from the injection site (Figure 4E, red arrowheads).

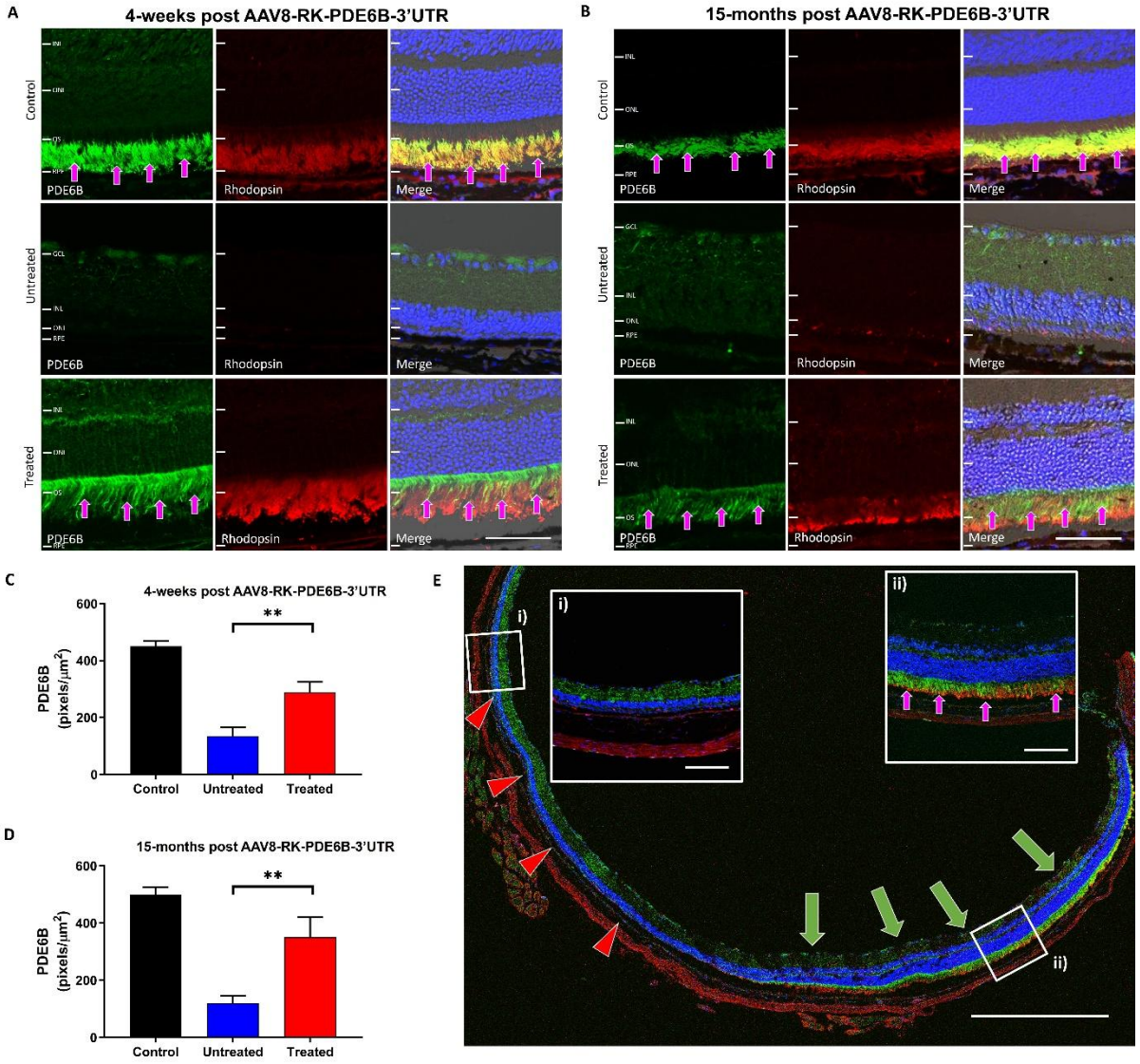


Figure 4: Increased PDE6B expression and photoreceptor rescue in *rd10* AAV8-RK-PDE6B-3'UTR treated retina. (A) Representative multi-marker immunohistochemistry of retinal sections from Control, Untreated and Treated conditions at 4 weeks and (B) 15 months post-treatment, immunostained for PDE6B (PDE6B; green, indicated by the up pink arrows) and rod photoreceptors (Rhodopsin; red). Nuclei are Hoechst-stained (blue). The 'Merge' panel encompasses all the stains

with bright-field. The untreated retina lacked photoreceptors as the condition displayed neither PDE6B or rhodopsin immunoreactivity at both timepoints. In the treated retina (AAV8-RK-PDE6B-3'UTR construct) there was strong immunolabelling of PDE6B in the rhodopsin-labelled photoreceptor outer segments, comparable to the control retina. Scale bar = 100 μm. GCL, ganglion cell layer; INL, inner nuclear layer; ONL, outer nuclear layer; OS, photoreceptor layer outer segment; RPE, retinal pigment epithelium. (C) Following AAV8-RK-PDE6B-3'UTR gene therapy, PDE6B expression in the OS layer (pixels/μm^2) was significantly increased at 4-weeks post-treatment and (D) and 15 months post-treatment. Significance relative to Untreated eyes (n = 5) is indicated as: **, $p < 0.01$. Error bar represents standard error mean. (E) Representative tile-scan image of the whole retinal section from a Treated condition at 4 weeks post-treatment. Areas of photoreceptor rescue (green arrows) with PDE6B expression are located near the site of injection of the AAV8-PDE6B-3UTR vector. Within the same eye, further away from the site of injection, there is an absence of photoreceptors and PDE6B expression (red arrowheads), along with retinal thinning. Scale bar = 500 μm. Magnification of areas away (inset: i)) and near (inset: ii)) site of injection of AAV8-RK-PDE6B-3'UTR construct are shown (green: PDE6B, red: rhodopsin, blue: Hoechst-stained nuclei). Scale bar = 100 μm. (Control: C57Bl/6 with no injection; Untreated: rd10 with no injection; Treated: rd10 with AAV8-RK-PDE6B-3'UTR injection).

PDE6B function was rescued and maintained in AAV8-RK-PDE6B-3'UTR treated *rd10* mice

To corroborate the expression of PDE6B expression with its function, cGMP immunohistochemistry was performed in treated *rd10* eyes. Functional rescue of PDE6B would result in a reduction in cGMP levels in the mouse retina. Consistent with this, the AAV8-RK-PDE6B-3'UTR treated *rd10* eyes displayed only weak staining of cGMP (within the outer nuclear layer and photoreceptor outer segment) at 15 months post- treatment, similar to wild-type C57Bl/6 (control) retinas, corresponding to the presence of functional PDE6B in these conditions (Figure 5A and B). Accumulation of cGMP in the photoreceptor outer segments is associated with non-functional or lack of PDE6B[5, 28], as was observed in P18 rd10 eyes (Figure 5C), which is more difficult to demonstrate at later ages because of marked photoreceptor degeneration in untreated eyes.

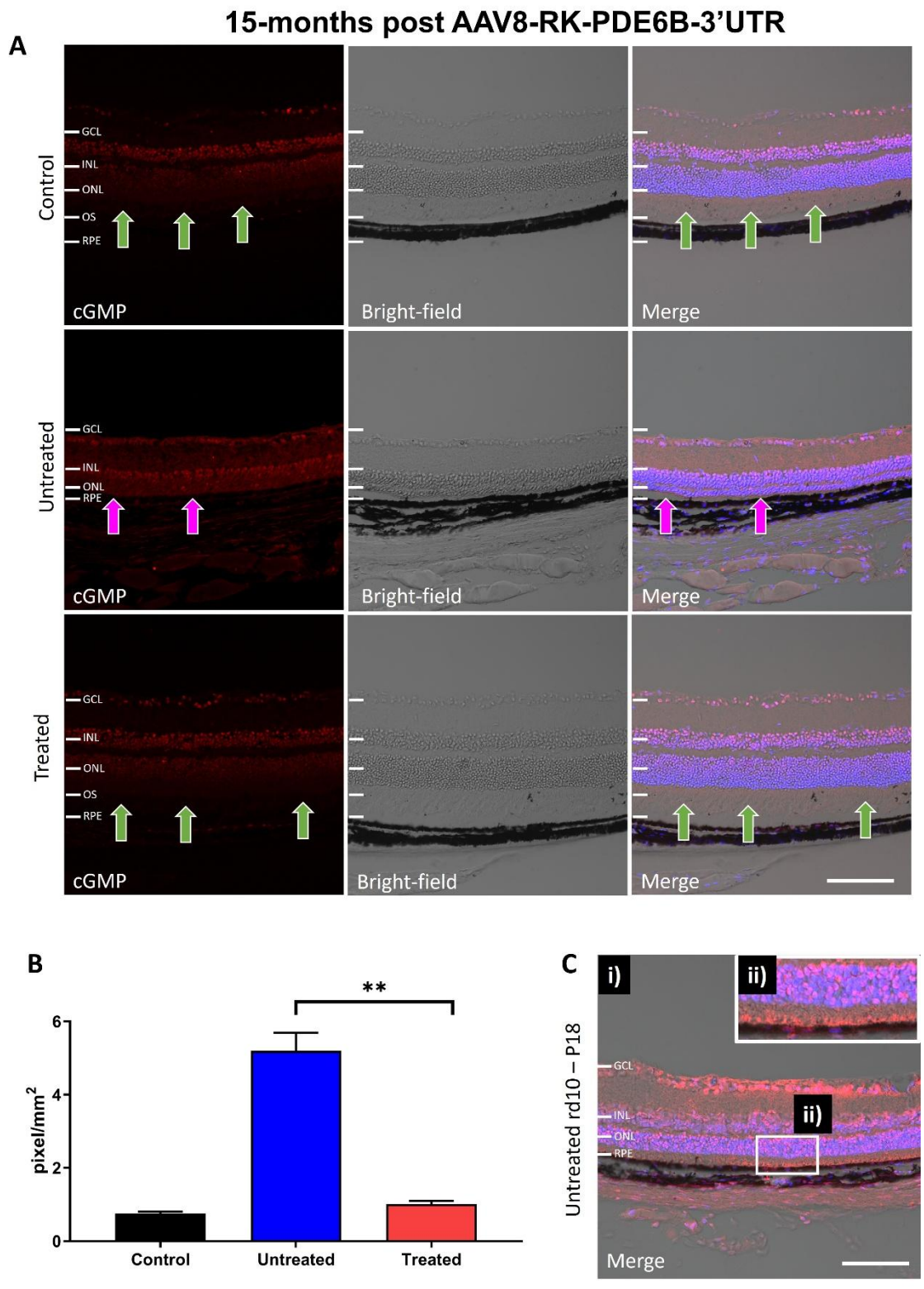
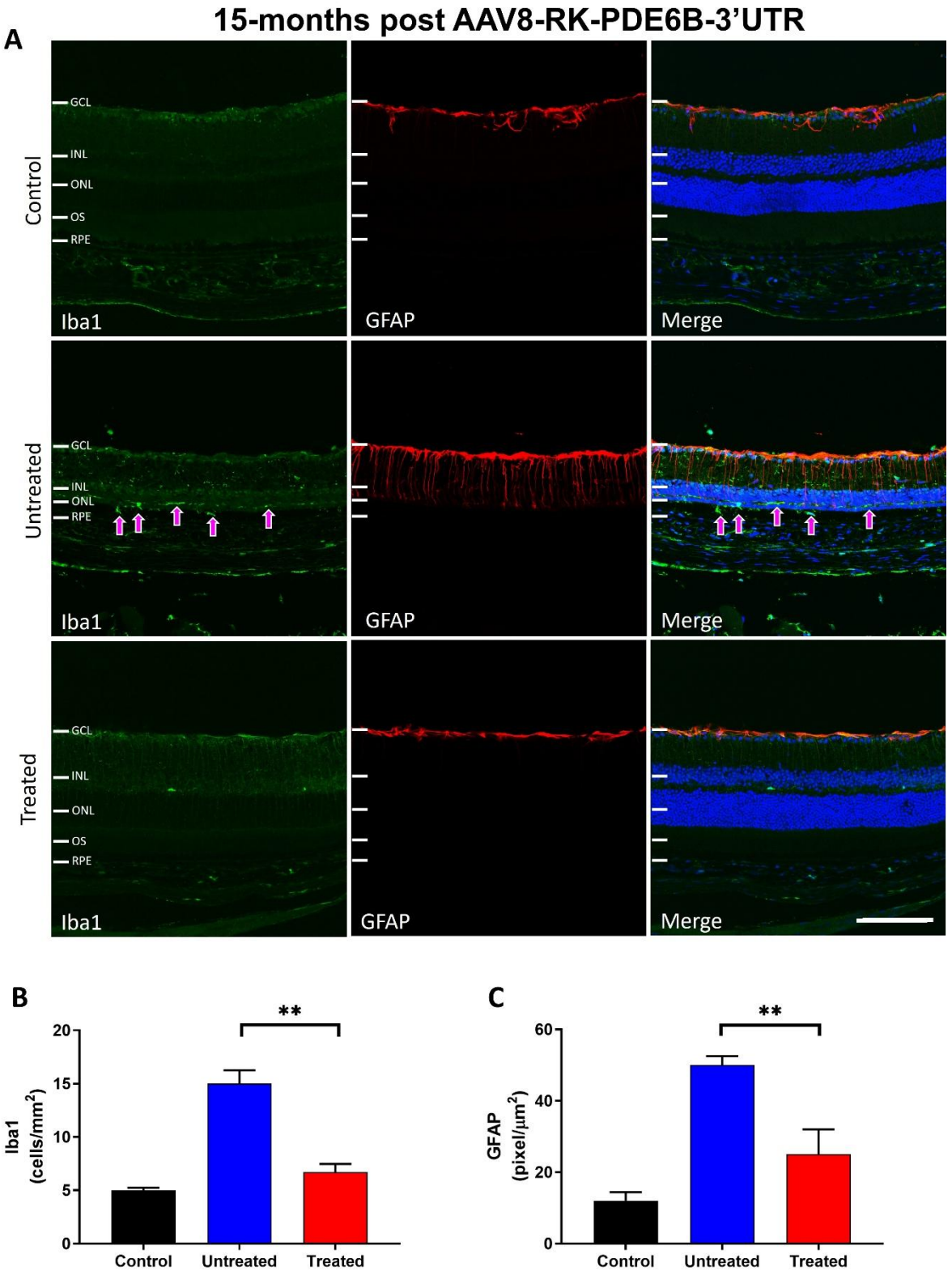


Figure 5: Functional PDE6B reduces cGMP accumulation in treated *rd10* retina. (A) Representative immunohistochemistry of retinal sections from Control, Untreated and Treated conditions at 15-months post-treatment time period, immunostained for

cGMP (cGMP; red). Nuclei are Hoechst-stained (blue). The 'Merge' panel encompasses all the stains with bright-field. In the treated retina, the ONL and OS of the photoreceptors can be seen via bright-field imaging and there was no accumulation of cGMP within the OS area, similar to the control retina (up green arrows). In the untreated retina, degeneration of the ONL and OS can be observed (up pink arrows), and overall thinning of the retina. Scale bar = 100 μm. GCL, ganglion cell layer; INL, inner nuclear layer; ONL, outer nuclear layer; OS, photoreceptor layer outer segment; RPE, retinal pigment epithelium. (B) At 15 months following AAV gene therapy (AAV8-RK-PDE6B-3'UTR construct) and with preservation of photoreceptors (as per Figure 4A), cGMP levels in the ONL and OS area (pixels/mm^2) were significantly reduced to levels similar to the Control condition, compared to elevated cGMP levels found in the Untreated condition, following normalisation to the area between the ONL and OS. Significance relative to Untreated *rd10* eyes (n = 5) is indicated as: **, $p < 0.01$. Error bar represents standard error mean. (C) Representative immunohistochemistry of a retinal section from Untreated condition at P18 (i)). Strong cGMP immunostaining within the ONL and OS area can be observed (white box inset). Scale bar = 100 μm. Magnification of area with cGMP accumulation within the ONL and OS (inset: ii)) are shown. (Control: C57Bl/6 with no injection; Untreated: rd10 with no injection; Treated: rd10 with AAV8-RK-PDE6B-3'UTR injection).

Reduced inflammatory cells and maintenance of cone photoreceptors and rod bipolar cells was evident in AAV8-RK-PDE6B-3'UTR treated *rd10* mice

Retinal cross-sections were also examined with immunohistochemistry for inflammation-related cells (Iba1: microglia, GFAP: Müller glia) and other neuronal cells (cone arrestin: cone photoreceptors, PKCα: rod bi-polar cells). At 4 weeks post-treatment we found that Iba1 microglia density in the Untreated and Treated condition remained high compared to C57Bl/6 control conditions (Suppl Fig 1A and B). In addition to the increase in numbers, the microglia also exhibited a largely activated (amoeboid) morphology with extensive dendritic branches infiltrating from the INL into the ONL[29]. In contrast, at 15 months post AAV8-RK-PDE6B-3'UTR, the Treated condition showed lower Iba1 cell density (Figure 6A and B) similar to levels observed in the Control condition. For the Untreated condition, increased microglia density and activated morphology were consistently observed up to the 15 month time period.



466

467 **Figure 6: Reduced microglia and glial expression in *rd10* retina treated AAV8-**
468 **RK-PDE6B-3'UTR vector.** (A) Representative multi-marker immunohistochemistry of
469 retinal sections from Control, Untreated and Treated conditions at 15 month time

period, immunostained for microglia (Iba1; green) and activated Müller glia (GFAP; red). Nuclei are Hoechst-stained (blue). The 'Merge' panel encompasses all the stains. The untreated retina exhibited increase microglia density and activation, indicative from the presence of microglia infiltrating into the ONL (up pink arrows), as well as extension of Müller glia processes from the GCL to ONL. Microglia and Müller glia activation was circumvented in the treated retina (AAV8-RK-PDE6B-3'UTR construct) following AAV gene therapy. Scale bar = 100 μm. GCL, ganglion cell layer; INL, inner nuclear layer; ONL, outer nuclear layer; OS, photoreceptor layer outer segment; RPE, retinal pigment epithelium. (B) At the 15-month time point, a significant decrease in cell density (cells/mm^2; region = between GCL to RPE layer) of microglia was observed in the treated retina. (C) Similarly, glial activation (pixel/μm^2; region = between GCL to RPE layer) was substantially reduced in the treated retina, 15 months post injection. Significance relative to Untreated eyes (n = 5) is indicated as: **, $p < 0.01$. Error bar represents standard error mean (Control: C57Bl/6 with no injection; Untreated: rd10 with no injection; Treated: rd10 with AAV8-RK-PDE6B-3'UTR injection).

Similarly, at 4 weeks post-treatment, we found that GFAP expression (Suppl Fig 1A and C) was significantly higher in both the Untreated and Treated conditions compared to Control. However, this was mitigated at the 15 month time period as the Treated condition showed significantly lower GFAP Müller glia staining, comparable to Control levels (Figure 6A and C).

493 Loss of Cone-arrestin^{+} cone photoreceptors and thinning of the retina was observed
494 in the Untreated condition but these cells and retinal thickness were maintained
495 following AAV8-PDE6B-3'UTR therapy (Figure 7A, B) at 15 months post-treatment
496 (Figure 7A, B). Similarly, PKCα^{+} rod bi-polar cells were observed to be highly
497 dysmorphic and disorganised in the Untreated condition but retained normal
498 morphology and lamination in the Treated condition (Figure 7A) at 15 months post-
499 treatment (Figure 7A, C).

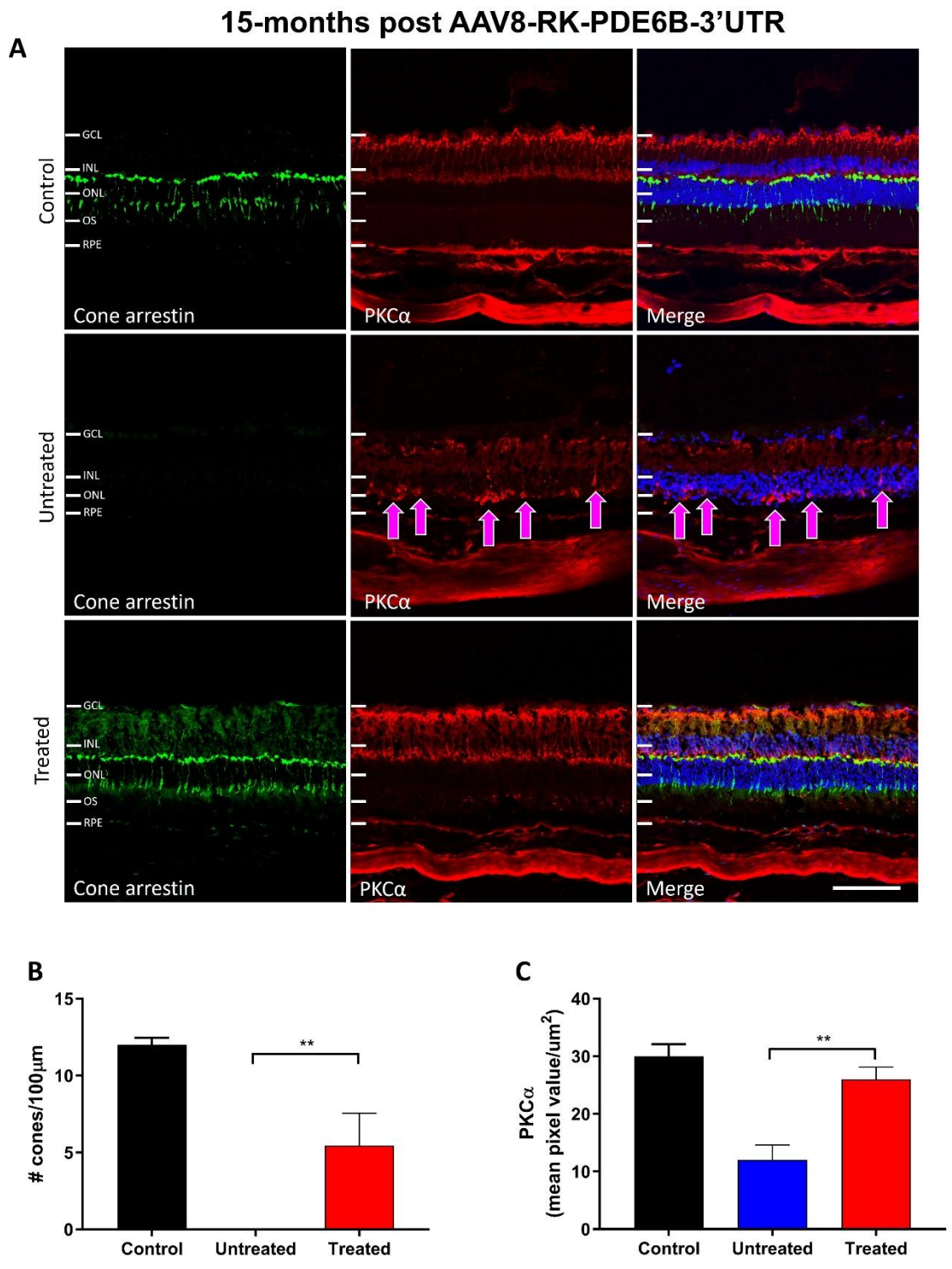


Figure 7: Cone photoreceptor and rod bi-polar cell preservation in treated *rd10* retina. (A) Representative multi-marker immunohistochemistry of retinal sections from Control, Untreated and Treated conditions at 15 month time period, immunostained for cone photoreceptors (Cone arrestin; green) and rod bi-polar cells (PKCα; red).

Nuclei are Hoechst-stained (blue). The 'Merge' panel encompasses all the stains. Complete absence of cone photoreceptors was observed in the untreated retina, corresponding to degeneration of the PL. Spatial distribution and synaptic termini of rod-bipolar cells were perturbed and appeared dysmorphic in untreated eyes (pink arrows). In the treated retina (AAV8-RK-PDE6B-3'UTR construct), cone photoreceptors were well preserved, and rod-bipolar cells remained laminated and maintained their synaptic contacts in the plexiform between INL and ONL. These patterns were similar to the control retina. Scale bar = 100 μm. GCL, ganglion cell layer; INL, inner nuclear layer; ONL, outer nuclear layer; OS, photoreceptor layer outer segment; RPE, retinal pigment epithelium. (B) At the 15-month time point in the treated retina, cone photoreceptors were preserved in the area of rescue (cones/100 μm) compared to the complete degeneration of cones observed in the untreated retina. (C) Similarly, rod bi-polar cell integrity (pixel/μm^2; region = between GCL to ONL layer) was maintained in the treated retina, 15 months post injection. Significance relative to Untreated eyes (n = 5) is indicated as: **, $p < 0.01$. Error bar represents standard error mean (Control: C57Bl/6 with no injection; Untreated: rd10 with no injection; Treated: rd10 with AAV8-RK-PDE6B-3'UTR injection).

Discussion

This study demonstrated long-term restoration of vision and maintenance of retinal structure and photoreceptor integrity with an AAV8-RK-PDE6B-3'UTR gene therapy construct in *rd10* mice. While there are other genetic therapy approaches reported in animal models of *PDE6B*-related retinitis pigmentosa [14, 30-35], and one gene addition approach, now terminated, was in phase I/II clinical trial using the AAV2/5 capsid (ClinicalTrials.gov Identifier: NCT03328130, registration date 1 November 2017), there is no current clinical therapy available for human patients. In this project, we sought to optimise a gene addition approach as the majority of pathogenic and likely pathogenic *PDE6B* variants cause disease through a loss-of-function (ClinVar, NCBI) disease mechanism, so an optimised gene addition approach would provide a therapeutic avenue for the majority of affected individuals.

3'UTR and RK promoter sequence enhanced PDE6B gene augmentation therapy

To date, many different AAV serotypes have been successfully used in preclinical and clinical studies in IRD, especially AAV5 and AAV8[12, 13]. Several studies have found that AAV8 was able to confer higher photoreceptor transduction efficiency, and stable transgene expression, in mice, dogs, nonhuman primate animal models, and retinal cellular models, compared with AAV2/2 and AAV2/5[9, 10, 35-38]. Hence, in our study we used AAV8.

Besides capsid consideration, the packaged construct with the gene of interest must be optimised and amenable to reflect the IRD model, due to packaging size limitations. Cellular heterogeneity within the retina necessitates the need for a defined cell-specific

promoter. The human rhodopsin kinase, also known as G protein-coupled receptor kinase 1 (hGRK1)[39], promoter was found to successfully drive expression in photoreceptors in mice, dogs, non-human primates and humans[40-42]. Currently, there are ongoing Phase I/II and II/III gene therapy trials targeting RP that utilise the hGRK1 promoter in their AAV construct[11, 43]. Our construct utilised the long form of the hGRK1 promoter, based on Beltran *et al*.[44], and we successfully showed specific and stable PDE6B expression in mouse photoreceptor cells up to 15 months post-injection.

One of the key regulators that can promote gene expression is the inclusion of post-transcriptional regulatory elements in the gene cassette[11, 16]. Some examples of these can be found upstream of the promoter sequence in the 5'UTR region (5'UTR), in the protein coding region, and the 3'UTR including the polyadenylation (PolyA) signal[11, 16]. These elements may provide stability for the mRNA structure during translation, promotion of transcriptional complex formation and enhanced protein activity [15, 41, 45]. Synthetic 5'UTRs were reported to enhance protein expression[15] particularly in muscle cell types. An alternative was 3'UTR, which was found to regulate mRNA stability, localisation and translation[46] and this was also found for PDE6B[47]. Interestingly, Sangermano *et al*. reported a pathogenic variant in *PDE6B* due to deletion in the 3'-UTR region in a patient with early onset rod-cone degeneration, highlighting the functional importance of this region for optimum *PDE6B* expression [48]. In view of this, we used the PDE6B 3'UTR region in our construct, which had a positive impact on PDE6B expression over and above this increased expression simply being due to optimal size for AAV packaging (Figure 1, A – E). Our *in vitro* and *in vivo* screening results demonstrated that the PDE6B therapy construct with 3'UTR resulted in the greatest PDE6B expression and rescue effect.

572

573 Beltran *et al*. found that doses of AAV5-hGRK1-GFP above 7.05 x 10^{10} GC, delivered
574 subretinally in a canine model, resulted in outer nuclear layer thinning and cone
575 photoreceptor toxicity[44]. In our study, we delivered 1.8 x 10^{10} GC of AAV8-RK-PDE6B-
576 3'UTR subretinally and found it to be well tolerated in *rd10* mouse retina as we
577 observed no structural compromise, and the retinal layers in the area of rescue
578 remained well laminated and phototransductive.

579

580 **Expression of PDE6B in rescued rod photoreceptors and maintenance of cone**
581 **photoreceptors and second order neurons**

582 We were able to demonstrate expression of PDE6B within rhodopsin$^+$ rod
583 photoreceptors, following delivery of our AAV8-RK-PDE6B-3'UTR construct. We also
584 demonstrated that the PDE6B protein was functionally competent during
585 phototransduction, as the rescued photoreceptors did not show accumulation of
586 cGMP, as compared to photoreceptors in untreated young *rd10* mice, hence
587 preventing the associated perturbed cellular calcium homeostasis which may lead to
588 eventual photoreceptor degeneration[5].

589

590 In our study, we found that restoration of rods was associated with prevention of death
591 of cone photoreceptors, as there was a substantial amount of C-arrestin$^+$ cones within
592 the treated *rd10* mice eyes. In all forms of RP, the visual symptoms involve the loss of
593 achromatic night vision, followed by loss of central vision acuity, which is reflected in
594 the gradual degeneration of rods where the genetic mutation is exclusively expressed

595 in, and then secondary death of cones[49,50]. The degeneration of cones could be
596 attributed to many factors including loss of trophic factors produced by rod
597 photoreceptors, and rod-death related initiation of oxidative stress, cytotoxin release,
598 and microglia activation[50]. The presence of healthy rod and cone photoreceptors in
599 our treated condition was corroborated by both VA and ERG testings, as the treated
600 *rd10* mice exhibited significant improvements in both functional areas. These changes
601 of scotopic and photopic responses in our study correlate well with the OCT data and
602 morphological structural changes in the retina, whereby in the untreated condition
603 there was complete retinal thinning and remodelling compared to treated retina.
604 Typically, the area around the site of injection exhibited photoreceptor rescue which
605 represents 1/3 of the whole retina. Consequently, the dark- and light-adapted B-wave
606 amplitudes in our Treated condition at 15 months were 30 – 40%, respectively of the
607 amplitudes of C57Bl/6 control conditions. Our results correspond to similar rescue
608 effects in previous investigations of rd1[34] and rd10[14] mouse models, with our study
609 showing longer term maintenance timepoints of rescue than these and other previous
610 studies. Long-term validation of therapeutic efficacy is crucial due to reports of IRD
611 gene therapy clinical studies showing decreased visual sensitivity, and photoreceptor
612 deterioration in patients within 3 years of receiving the therapy construct[20, 51].

613

614 Retinal degeneration not only affects photoreceptors but also second-order neurons
615 in the retinal circuitry, including bipolar and horizontal cells, causing them to remodel
616 their synaptic connections, display early retraction and loss of dendrites, and become
617 deafferent[52, 53]. In our untreated *rd10* retina, we observed substantial reduction in rod-
618 bipolar cells and the morphology was completely disorganised, indicating the

dependence of other secondary neuronal cells within the retina on photoreceptor presence. In a *rd10* model, it was found that loss of synaptic connections with photoreceptors evoked connective re-patterning in rod bipolar post-synaptic cells, followed by axonal atrophy, disrupted cell body lamination pattern, and eventual death[52]. We found that restoration of the photoreceptors in our system also preserved the integrity of PKCα^{+} rod-bipolar cells, with elaborated processes extending from the ganglion cell layer towards the photoreceptor synaptic terminal in the ONL. These morphological changes in the rod bipolar cells are reflected in the changes of scotopic and photopic B-wave amplitudes in our treated and untreated conditions, functionally validating the therapeutic effect on secondary neurons.

Gene replacement therapy mitigates inflammatory effects following RP rescue

Microglia play a key role in the CNS and retina system, including inflammatory and immune response modulation, scavenging pathogens, and phagocytosing cellular debris[54]. We observed a significant increase in the number of activated Iba1^{+} microglia cells in the retina of the untreated *rd10* mice, consistent with other studies that have observed a strong association of microglia recruitment in various retinal degenerative conditions such as age-related macular degeneration (AMD) and RP[27, 55]. The presence of microglia has been implicated in the pathogenesis of RP with peak microglia activation found to coincide during the occurrence of greatest photoreceptor death in RP[56]. As such, other studies have reported that activated microglia can further potentiate photoreceptor cell death in AMD, glaucoma or RP, either by phagocytosis or release of cytotoxic factors[54, 55]Here, we were able to show that in the treated *rd10* mice retina, at 15 months post-gene augmentation therapy, there was reduced

643 microglia cell density and decreased dendritic morphological processes, indicative of
644 successful photoreceptor rescue, and that the delivery of the AAV gene therapy
645 construct did not result in long term adverse retinal inflammation.

646

647 Hypertrophy of Müller glia processes within the retina is known to be associated with
648 various retinal degenerative conditions such as AMD, diabetic retinopathy and RP[27,
649 57, 58]. Typically, Müller glia cells respond to insults to the retina through gliosis and
650 upregulation of the intermediate filament protein, GFAP[59]. Mowat *et al*. found that
651 GFAP was significantly lower following gene augmentation therapy of PDE6A in a
652 canine model of retinitis pigmentosa [60]. Consistent with these findings, we showed
653 increased GFAP immunoreactivity associated with Müller glia spatial distribution in
654 untreated RP retinas which coincided with areas of photoreceptor atrophy (Figure 6A).
655 While inflammatory responses were present 4 weeks post-treatment in our study
656 which may have been due to initial loss of some photoreceptors, they were not present
657 at 15 months post treatment, suggesting that the photoreceptor rescue at 15 months
658 post treatment was sufficient to prevent long-term inflammatory responses.

659

660 Our study addresses the need for long-term gene therapy assessment by
661 demonstrating sustained functional rescue in an RP mouse model 15 months post-
662 treatment, evidenced by preserved retinal cytoarchitecture, stable electrophysiology,
663 normal cGMP levels, and reduced inflammation. This was achieved through
664 optimisation of our AAV vector construct including addition of PDE6B 3'UTR
665 sequence, to enable sustained and efficient expression and transduction of human
666 PDE6B in rod photoreceptors. Taken together, our results suggest that the therapeutic

efficacy we reported here, using our AAV vector construct, would translate to long-term therapeutic efficacy in clinical trials.

Data Availability Statement

All pertinent data generated and analysed during this study can be found within the published manuscript and supplementary data file.

References

1. Carss KJ, Arno G, Erwood M, Stephens J, Sanchis-Juan A, Hull S *et al.* Comprehensive Rare Variant Analysis via Whole-Genome Sequencing to Determine the Molecular Pathology of Inherited Retinal Disease. *Am J Hum Genet* 2017; **100**(1)**:** 75-90.

2. Khateb S, Nassisi M, Bujakowska KM, Mejecase C, Condroyer C, Antonio A *et al.* Longitudinal Clinical Follow-up and Genetic Spectrum of Patients With Rod-Cone Dystrophy Associated With Mutations in PDE6A and PDE6B. *JAMA Ophthalmol* 2019; **137**(6)**:** 669-679.

3. Watson CJG, Nash BM, Loi TH, Grigg JR, Jamieson RV. Genetic Variants and Impact in PDE6B Rod-Cone Dystrophy. In: Prakash G, Iwata T (eds). *Advances in Vision Research, Volume III: Genetic Eye Research around the Globe*. Springer Singapore: Singapore, 2021, pp 197-206.

4. Doonan F, Donovan M, Cotter TG. Activation of multiple pathways during photoreceptor apoptosis in the rd mouse. *Invest Ophthalmol Vis Sci* 2005; **46**(10)**:** 3530-8.

5. Xu J, Morris L, Thapa A, Ma H, Michalakis S, Biel M *et al.* cGMP accumulation causes photoreceptor degeneration in CNG channel deficiency: evidence of cGMP cytotoxicity independently of enhanced CNG channel function. *J Neurosci* 2013; **33**(37)**:** 14939-48.

6. Gargini C, Terzibasi E, Mazzoni F, Strettoi E. Retinal organization in the retinal degeneration 10 (rd10) mutant mouse: a morphological and ERG study. *J Comp Neurol* 2007; **500**(2)**:** 222-38.

7. Veleri S, Lazar CH, Chang B, Sieving PA, Banin E, Swaroop A. Biology and therapy of inherited retinal degenerative disease: insights from mouse models. *Dis Model Mech* 2015; **8**(2)**:** 109-29.

8. Trapani I, Puppo A, Auricchio A. Vector platforms for gene therapy of inherited retinopathies. *Prog Retin Eye Res* 2014; **43:** 108-28.

9. Hickey DG, Edwards TL, Barnard AR, Singh MS, de Silva SR, McClements ME *et al.* Tropism of engineered and evolved recombinant AAV serotypes in the rd1 mouse and ex vivo primate retina. *Gene Ther* 2017; **24**(12)**:** 787-800.

10. Vandenberghe LH, Bell P, Maguire AM, Cearley CN, Xiao R, Calcedo R *et al.* Dosage thresholds for AAV2 and AAV8 photoreceptor gene therapy in monkey. *Sci Transl Med* 2011; **3**(88)**:** 88ra54.

11. Buck TM, Wijnholds J. Recombinant Adeno-Associated Viral Vectors (rAAV)-Vector Elements in Ocular Gene Therapy Clinical Trials and Transgene Expression and Bioactivity Assays. *Int J Mol Sci* 2020; **21**(12).

12. Campochiaro PA, Avery R, Brown DM, Heier JS, Ho AC, Huddleston SM *et al.* Gene therapy for neovascular age-related macular degeneration by subretinal delivery of RGX-314: a phase 1/2a dose-escalation study. *Lancet* 2024; **403**(10436)**:** 1563-1573.

13. Hinsch VG, Boye SL, Boye SE. A Comprehensive Review of Clinically Applied Adeno-Associated Virus-Based Gene Therapies for Ocular Disease. *Hum Gene Ther* 2025; **36**(19-20)**:** 1301-1320.

14. Pang JJ, Dai X, Boye SE, Barone I, Boye SL, Mao S *et al.* Long-term retinal function and structure rescue using capsid mutant AAV8 vector in the rd10 mouse, a model of recessive retinitis pigmentosa. *Mol Ther* 2011; **19**(2)**:** 234-42.

15. Cao J, Novoa EM, Zhang Z, Chen WCW, Liu D, Choi GCG *et al.* High-throughput 5' UTR engineering for enhanced protein production in non-viral gene therapies. *Nat Commun* 2021; **12**(1)**:** 4138.

16. Naso MF, Tomkowicz B, Perry WL, 3rd, Strohl WR. Adeno-Associated Virus (AAV) as a Vector for Gene Therapy. *BioDrugs* 2017; **31**(4)**:** 317-334.

17. Pichard V, Provost N, Mendes-Madeira A, Libeau L, Hulin P, Tshilenge KT *et al.* AAV-mediated Gene Therapy Halts Retinal Degeneration in PDE6beta-deficient Dogs. *Mol Ther* 2016; **24**(5)**:** 867-76.

18. Ducloyer J-B, Le Meur G, Lebranchu P, BILLAUD F, Giraud L, Meunier S *et al.* 12-Month Safety and Efficacy Evaluation of HORA-PDE6B, a Gene Therapy Targeting Patients with Retinitis Pigmentosa Due to Biallelic PDE6B Gene Mutation. *Investigative Ophthalmology & Visual Science* 2024; **65**(7)**:** 2134-2134.

19. Fischer MD, Simonelli F, Sahni J, Holz FG, Maier R, Fasser C *et al.* Real-World Safety and Effectiveness of Voretigene Neparvovec: Results up to 2 Years from the Prospective, Registry-Based PERCEIVE Study. *Biomolecules* 2024; **14**(1).

20. Jacobson SG, Cideciyan AV, Roman AJ, Sumaroka A, Schwartz SB, Heon E *et al.* Improvement and decline in vision with gene therapy in childhood blindness. *N Engl J Med* 2015; **372**(20)**:** 1920-6.

21. Lee SHS, Chang H, Kim HJ, Choi JS, Kim J, Kim JH *et al.* Effects of Stuffer DNA on the Suppression of Choroidal Neovascularization by a rAAV Expressing a mTOR-Inhibiting shRNA. *Mol Ther Methods Clin Dev* 2019; **14:** 171-179.

22. Wu Z, Yang H, Colosi P. Effect of genome size on AAV vector packaging. *Mol Ther* 2010; **18**(1)**:** 80-6.

768 23. Strobel B, Miller FD, Rist W, Lamla T. Comparative Analysis of Cesium
769 Chloride- and Iodixanol-Based Purification of Recombinant Adeno-Associated
770 Viral Vectors for Preclinical Applications. *Hum Gene Ther Methods* 2015; **26**(4)**:**
771 147-57.

772

773 24. Tan E, Ding XQ, Saadi A, Agarwal N, Naash MI, Al-Ubaidi MR. Expression of
774 cone-photoreceptor-specific antigens in a cell line derived from retinal tumors
775 in transgenic mice. *Invest Ophthalmol Vis Sci* 2004; **45**(3)**:** 764-8.

776

777 25. Wagner JE, Schon C, Becirovic E, Biel M, Michalakis S. In Vitro Evaluation of
778 AAV Vectors for Retinal Gene Therapy. *Methods Mol Biol* 2019; **1834:** 383-390.

779

780 26. Ferguson LR, Grover S, Dominguez JM, 2nd, Balaiya S, Chalam KV. Retinal
781 thickness measurement obtained with spectral domain optical coherence
782 tomography assisted optical biopsy accurately correlates with ex vivo histology.
783 *PLoS One* 2014; **9**(10)**:** e111203.

784

785 27. Eamegdool SS, Sitiwin EI, Cioanca AV, Madigan MC. Extracellular matrix and
786 oxidative stress regulate human retinal pigment epithelium growth. *Free Radic*
787 *Biol Med* 2020; **146:** 357-371.

788

789 28. Lolley RN, Farber DB, Rayborn ME, Hollyfield JG. Cyclic GMP accumulation
790 causes degeneration of photoreceptor cells: simulation of an inherited disease.
791 *Science* 1977; **196**(4290)**:** 664-6.

29. Langmann T. Microglia activation in retinal degeneration. *J Leukoc Biol* 2007; **81**(6)**:** 1345-51.

30. Qin H, Zhang W, Zhang S, Feng Y, Xu W, Qi J *et al.* Vision rescue via unconstrained in vivo prime editing in degenerating neural retinas. *J Exp Med* 2023; **220**(5).

31. Wu Y, Wan X, Zhao D, Chen X, Wang Y, Tang X *et al.* AAV-mediated base-editing therapy ameliorates the disease phenotypes in a mouse model of retinitis pigmentosa. *Nat Commun* 2023; **14**(1)**:** 4923.

32. Su J, She K, Song L, Jin X, Li R, Zhao Q *et al.* In vivo base editing rescues photoreceptors in a mouse model of retinitis pigmentosa. *Mol Ther Nucleic Acids* 2023; **31:** 596-609.

33. Han IC, Wiley LA, Ochoa D, Lang MJ, Harman BE, Sheehan KM *et al.* Characterization of a novel Pde6b-deficient rat model of retinal degeneration and treatment with adeno-associated virus (AAV) gene therapy. *Gene Ther* 2023; **30**(3-4)**:** 362-368.

34. Nishiguchi KM, Carvalho LS, Rizzi M, Powell K, Holthaus SM, Azam SA *et al.* Gene therapy restores vision in rd1 mice after removal of a confounding mutation in Gpr179. *Nat Commun* 2015; **6:** 6006.

35. Petit L, Lheriteau E, Weber M, Le Meur G, Deschamps JY, Provost N *et al.* Restoration of vision in the pde6beta-deficient dog, a large animal model of rod-cone dystrophy. *Mol Ther* 2012; **20**(11)**:** 2019-30.

36. Dai X, He Y, Zhang H, Zhang Y, Liu Y, Wang M *et al.* Long-term retinal cone rescue using a capsid mutant AAV8 vector in a mouse model of CNGA3-achromatopsia. *PLoS One* 2017; **12**(11)**:** e0188032.

37. Du W, Tao Y, Deng WT, Zhu P, Li J, Dai X *et al.* Vitreal delivery of AAV vectored Cnga3 restores cone function in CNGA3-/-/Nrl-/- mice, an all-cone model of CNGA3 achromatopsia. *Hum Mol Genet* 2015; **24**(13)**:** 3699-707.

38. Gonzalez-Cordero A, Goh D, Kruczek K, Naeem A, Fernando M, Kleine Holthaus SM *et al.* Assessment of AAV Vector Tropisms for Mouse and Human Pluripotent Stem Cell-Derived RPE and Photoreceptor Cells. *Hum Gene Ther* 2018; **29**(10)**:** 1124-1139.

39. Young JE, Gross KW, Khani SC. Conserved structure and spatiotemporal function of the compact rhodopsin kinase (GRK1) enhancer/promoter. *Mol Vis* 2005; **11:** 1041-51.

40. Boye SE, Alexander JJ, Boye SL, Witherspoon CD, Sandefer KJ, Conlon TJ *et al.* The human rhodopsin kinase promoter in an AAV5 vector confers rod- and

cone-specific expression in the primate retina. *Hum Gene Ther* 2012; **23**(10)**:** 1101-15.

41. Khani SC, Pawlyk BS, Bulgakov OV, Kasperek E, Young JE, Adamian M *et al.* AAV-mediated expression targeting of rod and cone photoreceptors with a human rhodopsin kinase promoter. *Invest Ophthalmol Vis Sci* 2007; **48**(9)**:** 3954-61.

42. Weiss ER, Ducceschi MH, Horner TJ, Li A, Craft CM, Osawa S. Species-specific differences in expression of G-protein-coupled receptor kinase (GRK) 7 and GRK1 in mammalian cone photoreceptor cells: implications for cone cell phototransduction. *J Neurosci* 2001; **21**(23)**:** 9175-84.

43. Amato A, Arrigo A, Aragona E, Manitto MP, Saladino A, Bandello F *et al.* Gene Therapy in Inherited Retinal Diseases: An Update on Current State of the Art. *Front Med (Lausanne)* 2021; **8:** 750586.

44. Beltran WA, Boye SL, Boye SE, Chiodo VA, Lewin AS, Hauswirth WW *et al.* rAAV2/5 gene-targeting to rods:dose-dependent efficiency and complications associated with different promoters. *Gene Ther* 2010; **17**(9)**:** 1162-74.

45. Asrani KH, Farelli JD, Stahley MR, Miller RL, Cheng CJ, Subramanian RR *et al.* Optimization of mRNA untranslated regions for improved expression of therapeutic mRNA. *RNA Biol* 2018; **15**(6)**:** 756-762.

46. Mayr C. What Are 3' UTRs Doing? *Cold Spring Harb Perspect Biol* 2019; **11**(10).

47. Piri N, Mendoza E, Shih J, Yamashita CK, Akhmedov NB, Farber DB. Translational regulation of the rod photoreceptor cGMP-phosphodiesterase: the role of the 5'- and 3'-untranslated regions. *Exp Eye Res* 2006; **83**(4)**:** 841-8.

48. Sangermano R, Biswas P, Sullivan LS, Place EM, Borooah S, Straubhaar J *et al.* Identification of a novel large multigene deletion and a frameshift indel in PDE6B as the underlying cause of early-onset recessive rod-cone degeneration. *Cold Spring Harb Mol Case Stud* 2022; **8**(7).

49. Ferrari S, Di Iorio E, Barbaro V, Ponzin D, Sorrentino FS, Parmeggiani F. Retinitis pigmentosa: genes and disease mechanisms. *Curr Genomics* 2011; **12**(4)**:** 238-49.

50. Narayan DS, Wood JP, Chidlow G, Casson RJ. A review of the mechanisms of cone degeneration in retinitis pigmentosa. *Acta Ophthalmol* 2016; **94**(8)**:** 748-754.

51. Bainbridge JW, Mehat MS, Sundaram V, Robbie SJ, Barker SE, Ripamonti C *et al.* Long-term effect of gene therapy on Leber's congenital amaurosis. *N Engl J Med* 2015; **372**(20)**:** 1887-97.

52. Barhoum R, Martinez-Navarrete G, Corrochano S, Germain F, Fernandez-Sanchez L, de la Rosa EJ *et al.* Functional and structural modifications during retinal degeneration in the rd10 mouse. *Neuroscience* 2008; **155**(3)**:** 698-713.

53. Kalloniatis M, Nivison-Smith L, Chua J, Acosta ML, Fletcher EL. Using the rd1 mouse to understand functional and anatomical retinal remodelling and treatment implications in retinitis pigmentosa: A review. *Exp Eye Res* 2016; **150:** 106-21.

54. Zhao L, Zabel MK, Wang X, Ma W, Shah P, Fariss RN *et al.* Microglial phagocytosis of living photoreceptors contributes to inherited retinal degeneration. *EMBO Mol Med* 2015; **7**(9)**:** 1179-97.

55. Gupta N, Brown KE, Milam AH. Activated microglia in human retinitis pigmentosa, late-onset retinal degeneration, and age-related macular degeneration. *Exp Eye Res* 2003; **76**(4)**:** 463-71.

56. Zeng HY, Zhu XA, Zhang C, Yang LP, Wu LM, Tso MO. Identification of sequential events and factors associated with microglial activation, migration,

and cytotoxicity in retinal degeneration in rd mice. *Invest Ophthalmol Vis Sci* 2005; **46**(8)**:** 2992-9.

57. Kielczewski JL, Hu P, Shaw LC, Li Calzi S, Mames RN, Gardiner TA *et al.* Novel protective properties of IGFBP-3 result in enhanced pericyte ensheathment, reduced microglial activation, increased microglial apoptosis, and neuronal protection after ischemic retinal injury. *Am J Pathol* 2011; **178**(4)**:** 1517-28.

58. Roesch K, Stadler MB, Cepko CL. Gene expression changes within Muller glial cells in retinitis pigmentosa. *Mol Vis* 2012; **18:** 1197-214.

59. Bringmann A, Reichenbach A. Role of Muller cells in retinal degenerations. *Front Biosci* 2001; **6:** E72-92.

60. Mowat FM, Occelli LM, Bartoe JT, Gervais KJ, Bruewer AR, Querubin J *et al.* Gene Therapy in a Large Animal Model of PDE6A-Retinitis Pigmentosa. *Front Neurosci* 2017; **11:** 342.

Acknowledgements

We thank Professor Harry Steinbusch and Doctor Jan de Vente at Maastricht University, The Netherlands, for provision of the cGMP antibody. The authors would also like to thank Professor Muayyad Al-Ubaidi at University of Houston, USA, for provision of the 661W cell line.

Author contributions

SSE and RVJ conceived of, designed, analysed data and wrote the manuscript. SSE, THL, AS, FCK, AC, and JRG acquired samples and helped perform experiments. THL, LL and IA provided reagents. All authors contributed to editing and approval of the final manuscript.

Funding

This work was funded in part by NHMRC grant GNT2013451 and Perpetual Impact grant IPAP 2021/1026 with support from Australian Vision Research, Cure Blindness Australia, Retina Australia, Neil and Norma Hill Foundation, Wilton Ainsworth and Luminesce Alliance – a not-for-profit joint venture between CMRI, the Sydney Children's Hospitals Network, and the Children's Cancer Institute and affiliated with the University of Sydney and the University of NSW.

Ethical Approval

948 Ethical approval from the Children's Medical Research Institute Animal Ethics
949 Committee (Project C205).

950

951 **Competing Interests**

952 The authors declare no competing interests.

953

Supplementary information

Table S1: QPCR primers used in this study.

Human PDE6B	**Forward**	5'- GACTCCGAGATCGTCTTCCCA -3'
	Reverse	5'- AGTGAGCTCGTCAGCAAATGA -3'
Mouse RNA pol	**Forward**	5'- CGAGAAGGTCTCATTGACACGG -3'
	Reverse	5'- ACCACCTGGTTGATGGAGTTCC -3'

Electroretinography

Electroretinogram (ERG) recordings were performed using a commercial platform (Ganzfeld ERG, Phoenix Research Laboratories, USA). For scotopic recordings, mice were dark adapted overnight prior to recording, and all procedures were performed under dim red light. Mice were anesthetised by injecting appropriate dose of intraperitoneal Ketamine/xylazine (0.1 ml/10 g body weight). The pupils of anesthetised mice were dilated using 0.5% tropicamide (Bausch & Lomb, Australia). A corneal electrode was placed in contact with the cornea covered with lubricant eye drops (Goniovisc 2.5%; Accutome, USA). The reference electrode was placed subcutaneously between the ears and the ground electrode inserted into the base of the tail. The mice were placed on a heated platform (Phoenix Research Laboratories, USA) during recording and recovery.

Scotopic ERGs were obtained for flashing green light of a range of intensities -1.7, -0.8, 0.1, 1, 1.9, 2.8, and 3.1 log cd sec/m^2). The number of sweeps and delay between

sweeps are given in Table S2. The electrical signals were analysed using LabScribe ERG software v3 version (iWorx Systems, USA).

Table S2: Green light settings for scotopic ERG at different flash intensities.

Green Stimuli (log cd sec/m^2)	Duration (ms)	Number of Sweeps	Delay between sweeps (sec)
-1.7	1	10	0.7
-0.8	1	10	0.7
0.1	1	10	0.7
1	1	10	0.7
1.9	1	10	10
2.8	1	5	20
3.1	1	5	20

For photopic ERG, the room light was turned on and the mouse eye was light adapted with green flash 3.1 log cd sec/m^2 for five minutes and the ERGs were obtained for flashing green and UV light of a range of intensities (-1.7, -0.8, 0.1, 1, 1.9, 2.8, and 3.1 log cd sec/m^2). The photopic ERG parameters are shown in Table S3. For both scotopic and photopic recordings, electroretinogram waveforms were averaged from 5 mice for each condition at each intensity level from 1 to 15 months post-injection.

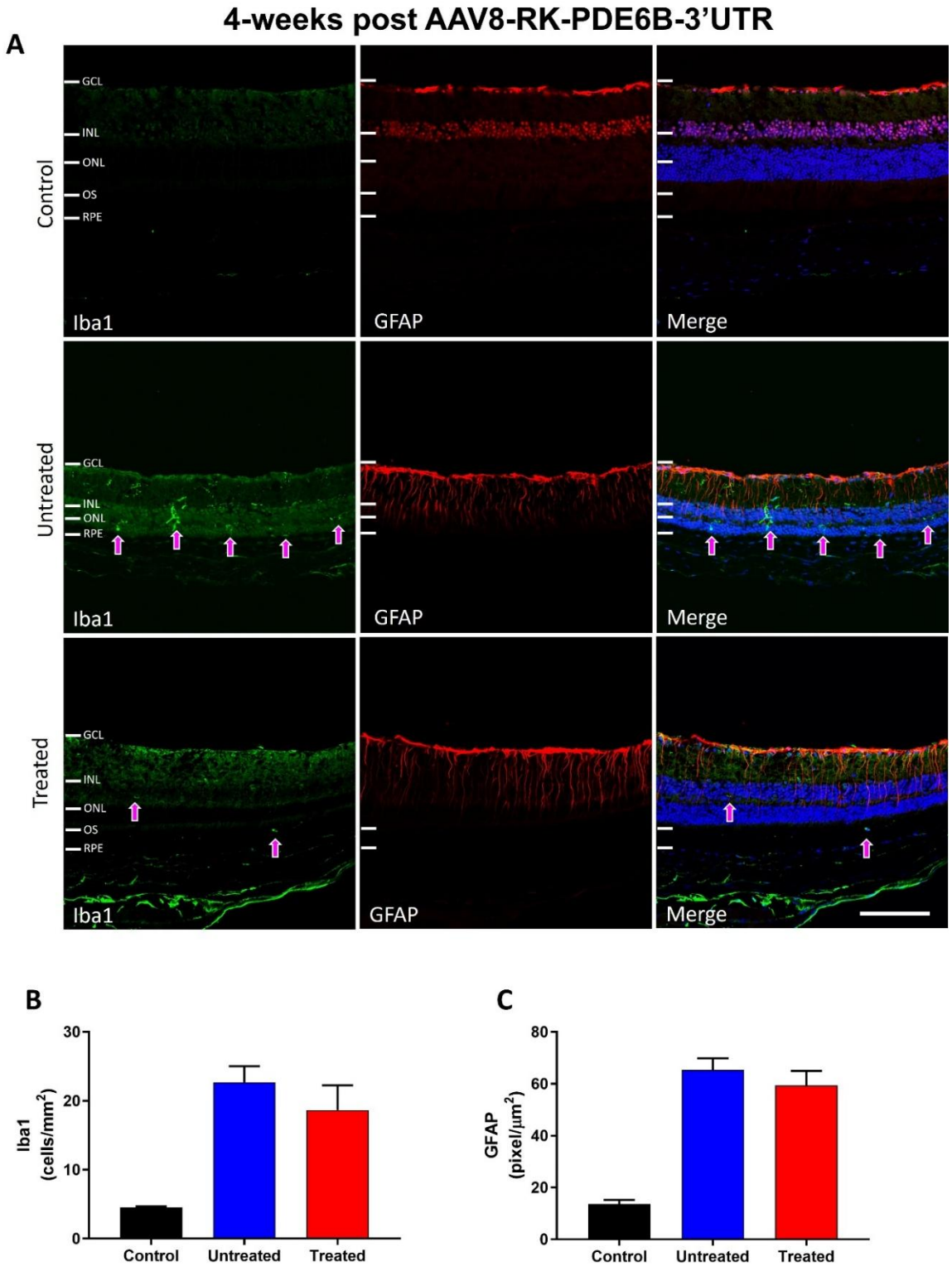
Table S3: Green and UV light settings for photopic ERG at different flash intensities.

Green Stimuli (log cd sec/m^2)	UV Stimuli (log cd sec/m^2)	Duration (ms)	Green Cont BG Light (log cd sec/m^2)	Number of Sweeps	Delay between sweeps (sec)
-1.7	-1.7	1	1.9	10	0.7
-0.8	-0.8	1	1.9	10	0.7
0.1	0.1	1	1.9	10	0.7
1	1	1	1.9	10	0.7
1.9	1.9	1	1.9	10	10
2.8	2.8	1	1.9	5	20

3.1	3.1	1	1.9	5	20

986

987



988

Supplementary Figure 1: Microglia and glial expression in *rd10* retina treated AAV8-PDE6B-3UTR vector at 4-weeks post-treatment. (A) Representative multi-marker immunohistochemistry of retinal sections from Control, Untreated and Treated conditions at 4-weeks time period, immunostained for microglia (Iba1; green) and activated Müller glia (GFAP; red). Nuclei are Hoechst-stained (blue). The 'Merge' panel encompasses all the stains. Both the untreated and treated retina exhibited increase microglia density and activation, indicative from the presence of microglia infiltrating into the ONL (up pink arrows), as well as Müller glia activation as seen from the GCL to ONL. Scale bar = 100 μm. GCL, ganglion cell layer; INL, inner nuclear layer; ONL, outer nuclear layer; OS, photoreceptor layer outer segment; RPE, retinal pigment epithelium. (B) At the 4-week time point, a significant amount of microglia remained in the treated retina (AAV8-RK-PDE6B-3'UTR construct). (C) Similarly, glial activation (pixel/μm^2) was present in the treated retina, 4-weeks post injection.

Supplementary Files

This is a list of supplementary files associated with this preprint. Click to download.

- SupplementarytablesWorddocformat.docx
- SupplementaryS1EamegdoolCMRI.tif